Fate of an electron beam in graphene: Coulomb relaxation or plasma instability?

Dmitry Svintsov*

Laboratory of 2d Materials for Optoelectronics, Moscow Institute of Physics and Technology, Moscow 141707, Russian Federation

(Received 24 October 2019; accepted 8 June 2020; published 25 June 2020)

Electron beams in two-dimensional systems can provide a useful tool to study energy-momentum relaxation of electrons and to generate microwave radiation stemming from plasma-beam instabilities. Naturally, these two applications cannot coexist: if instability exists, it strongly distorts the distribution function of beam electrons; if scattering is strong, it *typically* suppresses plasma instabilities. Here, we study the role of inevitable electron-electron (*e-e*) collisions on possible plasma beam instabilities in graphene and show that scattering effects are far less trivial. We find that an unstable plasma mode associated with beam bunching is stabilized already by weak *e-e* collisions. Quite surprisingly, further enhancement of *e-e* collisions results in loss compensation and self-excitation of an ordinary graphene plasmon mode. Such instability is interpreted as viscous transfer of momentum from an electron beam to two-dimensional plasmons. Its growth rate reaches its maximum at hydrodynamic-to-ballistic crossover, when plasmon wavelength and electron mean free path are of the same order of magnitude.

DOI: 10.1103/PhysRevB.101.235440

I. INTRODUCTION

The cornerstone of Landau Fermi liquid theory is weak scattering of a single electron excitation over the Fermi surface. The corresponding scattering rate due to electron-electron (*e-e*) collisions γ_{ee} is proportional to excitation energy squared $\delta\epsilon^2$ in three dimensions [1]. In reduced dimensions, the *e-e* scattering becomes stronger, which leads to non-Fermi-liquid behavior in one dimension [2] and log-enhanced scattering ($\sim\delta\epsilon^2 \ln|\delta\epsilon|/T$) in two dimensions [3]. Scattering among two-dimensional (2D) electrons has recently regained great attention [4] as it leads to novel fluidlike transport observed in numerous experiments [5–8].

While a single electron above the Fermi surface inevitably ends up with scattering, the fate of an electron bunch can be far more interesting. Namely, the appearance of a beam over the steady electron background results in a pair of new excitation modes with complex conjugate frequencies, one of which is unstable (growing) [9–11]. This phenomenon of plasma beam instability has been actively studied since the 1950s in connection with nuclear fission problem [12] and solar bursts [13].

The resurrection of interest to the fate of electron beams in 2D systems is dictated by two reasons. First, relaxation of the injected beam can provide valuable information on the rate of *e-e* scattering and its energy dependence that is challenging to access with other techniques [14–18]. Second, if the plasma-beam instability does indeed develop, the resulting oscillations can form the basis of solid-state terahertz sources [19–22]. Naturally, these two applications cannot coexist: plasma instability distorts the energy spectra of beam electrons hindering the determination of scattering mechanisms [23]. At the same time, strong scattering of beam electrons (*e-e* scattering being the unavoidable one) is generally believed to suppress the instabilities.

The idea of collisionless (ballistic) transport being the prerequisite of instability [19,20,22] was scarcely doubted, though real studies of beam instabilities in two dimensions in the presence of *e-e* collisions are lacking [24]. In this paper, we establish the criteria of beam instabilities and beam relaxation in graphene in the presence of *e-e* collisions of arbitrary strength.

First of all, we calculate the characteristics of instability associated with beam bunching in graphene (i.e., frequency and growth rate). We focus on importance of nonlocal effects in polarizability for correct determination of growth rate; such effects were ignored in preceding studies [25]. Quite expectantly, we find that already weak *e-e* scattering suppresses such instability. Further on, we find a new unexpected instability at the hydrodynamic-to-ballistic crossover where Knudsen number $\mathrm{Kn} = q v_0 \tau_{ee}$ is order of unity (q is the plasmon wave vector, v_0 is the Fermi velocity in graphene, and $\tau_{ee} = \gamma_{ee}^{-1}$ is mean time between *e-e* collisions). In this regime, the normal graphene plasmons become unstable in the presence of beam, while the physics of instability can be attributed to viscous momentum transfer between beam and collective modes. The effect of *e-e* collisions on collective modes in this regime is highly nonperturbative; still it can be handled analytically using model collision integrals [1,26,27]. While promotion of plasmon instabilities by *e-e* collisions looks counterintuitive, several such examples can be found in bulk Maxwellian plasmas [28].

The interest to graphene is motivated by the dominant role of *e-e* scattering in graphene-based heterostructures [7,29] due to low impurity density and high energy of optical phonons. In addition, formation of high-density electron beams with collimated velocities is easily achievable with graphene tunnel junctions [30,31] and geometrically patterned contacts [32,33].

*svintcov.da@mipt.ru

II. THEORY OF ELECTRON BEAM STABILITY IN GRAPHENE

In a canonical problem of plasma-beam instability, the electron beam in collimated in momentum space rather than in real space. The momentum collimation is readily achieved upon electron injection through tunnel junctions [30]. The angular distribution of tunnel-injected electrons is Gaussian, and its width shrinks with reducing the barrier transparency. In the following calculations, we shall mimic the distribution function of beam electrons as a delta function, $f_b(\mathbf{k}) = n_b\delta(\mathbf{k}-\mathbf{k}_b)$, where n_b is the density of injected electrons with momentum around $\mathbf{k}_b$ and the delta function is normalized according to $g(2\pi)^{-2}\int d^2\mathbf{k}\,\delta(\mathbf{k}-\mathbf{k}_b) = 1$ ($g = 4$ is the spin-valley degeneracy). The steady-state distribution function of electrons thus reads

$$f_0(\mathbf{k}) = f_F(\mathbf{k}) + n_b\delta(\mathbf{k}-\mathbf{k}_b), \tag{1}$$

where $f_F(\mathbf{k})$ is the Fermi function of background equilibrium electrons.

We are to analyze the electromagnetic stability of distributions (1). Such analysis is based on evaluation of dielectric function $\varepsilon(\mathbf{q},\omega)$ of an electron system followed by the search of unstable roots for plasmon dispersion relation $\varepsilon(\mathbf{q},\omega) = 0$. In turn, evaluation of dielectric function requires the knowledge of polarizability $\Pi(\mathbf{q},\omega)$ being the proportionality coefficient between induced electron density $\delta n_{\mathbf{q}\omega}$ and electric potential $\delta\varphi_{\mathbf{q}\omega}$, $\delta n_{\mathbf{q}\omega} = \Pi(\mathbf{q},\omega)e\,\delta\varphi_{\mathbf{q}\omega}$. The latter is found from a kinetic equation governing the electron distribution function f:

$$\frac{\partial f}{\partial t} + \mathbf{v}_\mathbf{k}\frac{\partial f}{\partial \mathbf{r}} + \frac{\partial V}{\partial \mathbf{r}}\frac{\partial f}{\partial \mathbf{k}} = \mathcal{C}_{ee}\{f\}. \tag{2}$$

Above, $\mathbf{v}_\mathbf{k} = v_0\mathbf{k}/k$ is the electron velocity in graphene and $V(\mathbf{r}) = -e\varphi(\mathbf{r})$ is the potential energy in electric field. The right-hand side is the electron-electron (e-e) collision integral.

To preserve the main features of e-e collisions and maintain analytical tractability, we adopt $\mathcal{C}_{ee}$ in the generalized relaxation-time approximation [26,27,34]. In this model, all perturbations of distribution function are relaxed toward local equilibrium

$$\mathcal{C}_{ee}\{f\} = \frac{f - f_{eq}}{\tau_{ee}}, \tag{3}$$

$$f_{eq}(\mathbf{k}) = \left[1 + \exp\left\{\frac{\varepsilon_\mathbf{k} - \mathbf{k}\mathbf{u}_{eq} - \mu_{eq}}{T_{eq}}\right\}\right]^{-1} \tag{4}$$

rather than to zero. Moreover, the parameters of this local equilibrium, which are quasi-Fermi level μ_{eq}, drift velocity $\mathbf{u}_{eq}$, and temperature T_{eq}, are different from those of steady background electrons. These parameters would be established after equilibration of background electron plasma and beam, and are determined from particle number, momentum, and energy conservation laws. If the density of beam electrons is small compared to equilibrium density n_0, the equilibrium drift velocity would be $u_{eq} \approx v_0(n_b/n_0)(k_b/k_F)$.

We further proceed to linearization of the Boltzmann equation with respect to small external potential $V(\mathbf{r}) = -e\,\delta\varphi_{\mathbf{q}\omega}e^{i(\mathbf{qr}-\omega t)}$. The distribution function acquires a correction $\delta f_{\mathbf{q}\omega}(\mathbf{k})e^{i\mathbf{qr}-i\omega t}$, and so does the local equilibrium function $f_{eq} = f_{eq}^{(0)} + \delta f_{eq}e^{i\mathbf{qr}-i\omega t}$. It is now possible to obtain a formal solution for $\delta f_{\mathbf{q}\omega}(\mathbf{k})$ (the subscript $\mathbf{q}\omega$ will be suppressed from now on):

$$\delta f(\mathbf{k}) = \frac{-\mathbf{q}\,e\delta\varphi\frac{\partial}{\partial\mathbf{k}}\{f_F(\mathbf{k}) + f_b(\mathbf{k})\} + i\gamma_{ee}\delta f_{eq}}{\omega + i\gamma_{ee} - \mathbf{q}\mathbf{v}_\mathbf{k}}. \tag{5}$$

Considerable precautions should be taken upon evaluation of momentum derivative for beam distribution function $\partial f_b(\mathbf{k})/\partial\mathbf{k}$. Once the beam distribution is delta peaked in momentum space, the derivative becomes ill defined. This problem is resolved if one recalls that Boltzmann kinetic equation is derived from the quantum Liouville equation in the quasiclassical limit [34]. This procedure is described in detail in Appendix A. Here, we provide only the resulting replacement rule for pathological terms (we set in the following $\hbar = 1$):

$$\frac{\mathbf{q}\partial f_b(\mathbf{k})/\partial\mathbf{k}}{\omega + i\gamma_{ee} - \mathbf{q}\mathbf{v}_\mathbf{k}} \to \frac{f_b(\mathbf{k}+\mathbf{q}) - f_b(\mathbf{k})}{\omega + i\gamma_{ee} - \epsilon_{\mathbf{k}+\mathbf{q}} + \epsilon_\mathbf{k}}, \tag{6}$$

where $\epsilon_\mathbf{k} = kv_0$ is the band dispersion in graphene.

The solution for the distribution function is accomplished after one finds the parameters of local-equilibrium function

$$\delta f_{eq} = \delta\mu\partial_\mu f_{eq}^{(0)} + \delta\mathbf{u}\partial_\mathbf{u} f_{eq}^{(0)} + \delta T\partial_T f_{eq}^{(0)}, \tag{7}$$

using the conservation laws upon collisions. More precisely, the time derivatives of particle number, momentum, and energy should turn to zero if collision integral (3) is evaluated on distribution functions (5) and (7). This procedure leads us to closed-form equations for local-equilibrium parameters $\delta\mu$, $\delta\mathbf{u}$, and δT. These can be called generalized hydrodynamic equations and are valid at an arbitrary value of Knudsen number $\mathrm{Kn} = qv_0\tau_{ee}$. The final form of these equations is quite cumbersome and presented in Appendix B, yet they yield simple results in hydrodynamic ($\mathrm{Kn} \ll 1$) and ballistic ($\mathrm{Kn} \gg 1$) limits.

III. RESULTS

A. Beam instability in graphene: Collisionless case

The polarization $\Pi(\mathbf{q},\omega)$ of an electron system with injected beam in the absence of collisions is the sum of individual contributions from steady electrons $\Pi_0(\mathbf{q},\omega)$ and the beam $\Pi_b(\mathbf{q},\omega)$. The dielectric function $\varepsilon(\mathbf{q},\omega)$ governing the collective response is therefore

$$\varepsilon = 1 + V_0[\Pi_0 + \Pi_b] \equiv \varepsilon_0 + V_0\Pi_b, \tag{8}$$

where we have introduced the Fourier transform of Coulomb potential in 2D $V_0 = 2\pi e^2/\kappa|q|$ (κ is the beackground dielectric constant), and dielectric function of equilibrium graphene electrons $\varepsilon_0 = 1 + V_0\Pi_0$.

The polarization of equilibrium electrons in the classical limit ($q \ll k_F, \omega \ll \varepsilon_F$) is given by (see [35] and Appendix A)

$$\Pi_0(q,\omega) = \frac{2}{\pi}\frac{k_F}{v_0}\left[1 - \frac{\omega}{\sqrt{(\omega+i0)^2 - q^2v_0^2}}\right]. \tag{9}$$

It is important that frequently adopted long-wavelength expansion of polarizability ($q \to 0$) may be applicable only for fast waves with phase velocity, $\omega/q \gg v_0$ [36]. We will see that unstable modes generated by beam are slow ($\omega/q < v_0$).

Therefore, the full form of polarization (9) should be used for stability analysis [37].

The beam polarization is given by

$$\Pi_b = n_b\left[\frac{1}{\omega-\omega_{b0}^-}-\frac{1}{\omega-\omega_{b0}^+}\right]. \tag{10}$$

It is proportional to the small density of beam electrons n_b, yet it is highly resonant in frequency. The poles of beam polarization are located at two beam-induced collective modes:

$$\omega_{b0}^{\pm} = \mathbf{q}\mathbf{v}_b \pm qv_0\sin^2\theta\frac{q}{2k_b}. \tag{11}$$

The frequency of these modes is *almost zero* in the reference frame of a beam, except for a small correction due to quantum effects. These quantum corrections are important to lift the degeneracy of beam-induced modes and correctly capture the low-density behavior of instability.

Interaction of beam with background electrons through self-consistent field results in modification of beam modes. Their frequencies are changed according to

$$\omega_b^{\pm} = \mathbf{q}\mathbf{v}_b \pm qv_0|\sin\theta|\left[\left(\frac{q\sin\theta}{2k_b}\right)^2+\frac{V_0(q)n_b/k_bv_0}{\varepsilon_0(\mathbf{q},\mathbf{q}\mathbf{v}_b)}\right]^{1/2}. \tag{12}$$

The beam-induced modes are no longer stable, independent of beam density n_b. Indeed, the dielectric function of graphene has a nonzero imaginary part at $\omega = \mathbf{q}\mathbf{v}_b < qv_0$, which signifies collisionless intraband absorption (Landau damping). The double sign before the square root in (12) implies that one mode (ω_b^+) is decaying while the other one (ω_b^-) is growing in time. The appearance of an unstable beam-induced mode is clearly seen in the plot of loss function $-\mathrm{Im}\epsilon^{-1}(q,\omega)$ in Fig. 1(a); the negative sign of loss function at the lowest mode implies its instability.

The instability growth rate depends on beam density linearly at small $n_b < n_0(q/k_b)$ and approximately as $n_b^{1/2}$ at larger values. The low-density limit can be described only with an account of quantum corrections to beam-induced modes.

The beam-induced modes always lie in the domain of intraband absorption $\omega < qv_0$, where the dielectric function of background electrons has a positive imaginary part, $\mathrm{Im}\varepsilon_0 > 0$ [as shown in Fig. 1(b)]. It may look counterintuitive that an absorptive dielectric function may give rise to plasmon gain, as it follows from Eq. (12). This is explained by the fact that the energy of electromagnetic oscillations $W(\mathbf{q},\omega)$ with frequency ω_b^- is negative [38]. The time derivative of oscillation energy is negative in absorptive media $dW(\mathbf{q},\omega)/dt < 0$, which corresponds to the growth of the absolute value of energy.

The plasmon gain appears in the thresholdless manner in the absence of *e-e* collisions, i.e., even a very small density of beam electrons gives rise to a proportionally small growth rate. Absence of threshold is inherited from the spatial dispersion of conductivity and resulting Landau damping. The thresholdless character of beam instability is not intrinsic to graphene; already in collisionless warm three-dimensional Maxwell plasma the Landau damping similarly gave rise to a beam instability [38]. However, reduction of temperature in the Maxwell plasma led to an exponential suppression of Landau damping. A special property of graphene and degenerate 2D electron systems in general is that Landau damping is never parametrically small, and cannot be neglected in the problem of beam instability.

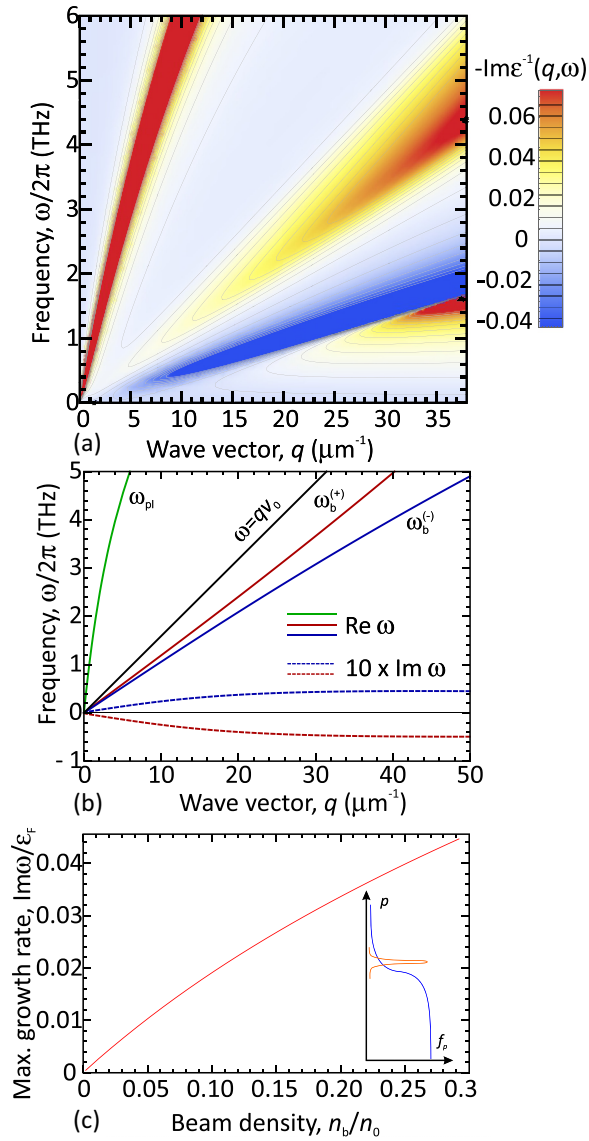

FIG. 1. Beam instability in a collisionless electron system in graphene. Panel (a) shows the calculated loss function $-\mathrm{Im}\varepsilon^{-1}(q,\omega)$ for graphene electrons with a beam in the ballistic regime. Fermi energy $\varepsilon_F = 100$ meV, beam density $n_b/n_0 = 0.1$, collision frequency $\hbar\gamma_{ee} = 600$ μeV, and $\kappa = 4$. Panel (b) shows the dispersion of normal plasmon (ω_{pl}, green line) and two beam-induced modes ($\omega_b^{\pm}$, red and blue lines). Dashed lines show the tenfold magnified damping and growth rates of beam-induced modes. Panel (c) shows the growth rate of a beam-induced mode (scaled by Fermi energy) maximized with respect to wave vector q and propagation angle θ. Inset shows the momentum distribution of electrons in the problem of beam instability.

It is possible to reveal the limiting values of instability growth rate with variation of wave vector q, propagation angle θ, and Coulomb interaction strength $\alpha_c = e^2/\kappa\hbar v_0$. A

close inspection of Eq. (12) shows that instability growth is favored by strong Coulomb interactions, i.e., $\mathrm{Im}\omega_b^-$ is a growing function of α_c. It reaches the maximum at the largest physically reasonable value $e^2/\hbar v_0 \approx 2.2$. For the same reason, instability in gated structures would be weaker, as the presence of gate at distance d effectively renormalizes $\alpha_c \to (e^2/\hbar\kappa v_0)(1-e^{-2|q|d})$. When varying the propagation angle θ and wave vector q, the growth rate reaches its maximum at $\theta \sim \pi/5$ and $q \sim k_F$. The result of constrained optimization of the beam instability growth rate with respect to q (in the range $q \in [0; k_F]$) and $\theta \in [0; \pi/2]$ is shown in Fig. 1(c) (see Appendix C for details).

We find that with a realistically small density of beam electrons $n_b/n_0 \approx 0.1$, the maximum achievable growth rate of beam instability is $\sim 0.02\varepsilon_F$. It becomes comparable to *e-e* collision frequency at temperatures $T \approx 0.1\varepsilon_F$. For realistic Fermi energy $\sim$100 meV, this corresponds to the liquid nitrogen temperature.

As the temperature is increased, *e-e* collisions destroy the ordinary beam instability. As far as the beam density is small ($n_b/n_0 \ll 1$) and collisions can be treated perturbatively ($\gamma_{ee} \ll \omega_b^{(\pm)}$), the effect of collisions is trivial and results in a shift of beam mode frequency by $-i\gamma_{ee}$. The in-scattering terms of collision integral can be neglected in this regime as they are proportional to the product of beam density and scattering rate. This result can be physically interpreted by smallness of phase space occupied by beam electrons, which results in low probability of electron scattering in the direction of beam propagation. Such a conclusion holds for an arbitrary model of *e-e* scattering and is not limited to the generalized relaxation time approximation analyzed here.

B. Excitation of graphene plasmons by injected electrons: Strong *e-e* collisions

The situation changes radically for *e-e* collisions with frequency comparable to that of plasmon modes. Numerically, it corresponds to terahertz frequencies in graphene at room temperature [39]. For ordinary plasmon modes in equilibrium with $\omega_{pl} \approx v_0\sqrt{4\alpha_c k_F q}$, this frequency range is characterized by strong viscous damping [27]. This result is illustrated in Fig. 2(b) with the red line. It shows that the damping rate of the bulk graphene plasmon vs *e-e* collision frequency has a maximum located at the crossover between ballistic and hydrodynamic regimes.

When the beam is injected into an electron plasma with strong *e-e* collisions, the maximum in the damping rate is transformed into the maximum of the growth rate, as shown in Fig. 2(b) with blue and black lines. The beam-induced modes are completely suppressed in this regime, as clearly seen in the plot of loss function for strong collisions in Fig. 2(a). We have verified that both plasmon damping and beam-induced instability disappear in the deep hydrodynamic regime ($\gamma_{ee} \to \infty$) and in the ballistic regime ($\gamma_{ee} \to 0$). Both effects appear as first-order corrections to plasmon dispersion in Knudsen number $\mathrm{Kn} = q v_0 \tau_{ee}$; in the absence of the beam the viscous damping equals $\omega'' = q v_0 \mathrm{Kn}/4$. The fact that beam-induced instability appears at the same order in Kn as viscosity enables us to interpret it as viscous momentum transfer between electron beam and normal plasmon modes.

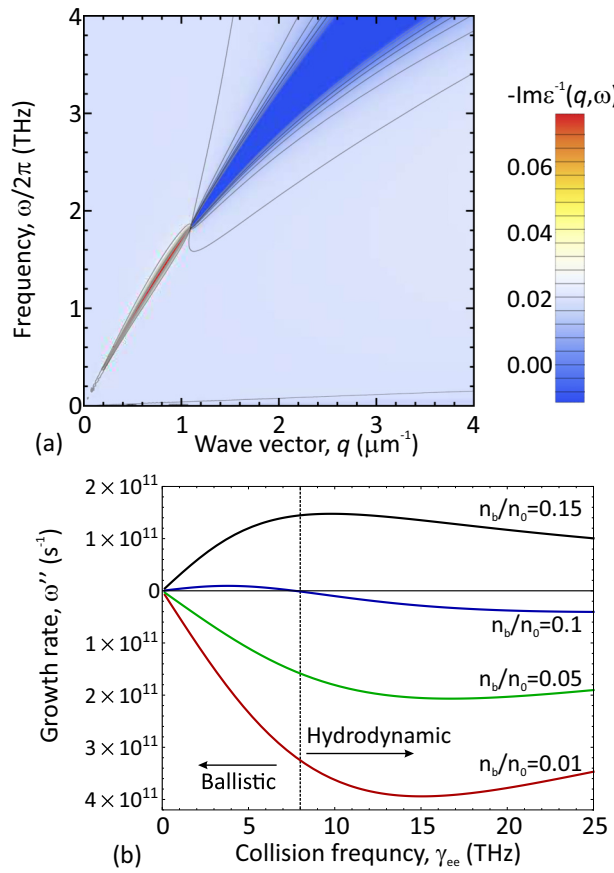

FIG. 2. Excitation of normal graphene plasmons by electron beam at the hydrodynamic-to-ballistic crossover. Panel (a) shows the calculated loss function $-\mathrm{Im}\varepsilon^{-1}(q,\omega)$ for graphene electrons with $\varepsilon_F = 150$ meV, beam density $n_b/n_0 = 0.095$, collision frequency $\hbar\gamma_{ee} = 25$ meV, and $\kappa = 4$. Panel (b) shows the calculated damping/growth rate of normal graphene plasmons vs e-e collision frequency at fixed wave vector $q = T/(\hbar v_0)$ and various densities of beam electrons. For small beam densities, the viscous damping reaches its maximum at $\mathrm{Kn} \sim 1$; for large beam densities so does the growth rate due to momentum transfer between beam and normal plasmon modes.

The growth rate of "normal" graphene plasmons due to viscous interaction with electron beam can be studied analytically by expansion of generalized hydrodynamic equations in the limit of small Knudsen number. Noting that the real part of normal plasmon frequency is almost unaffected by scattering, we can obtain the damping/growth rate as

$$\gamma = q v_0 \mathrm{Kn} \frac{\frac{m_{hd}}{m_b} P_1(s,\beta_{eq}) + P_2(s,\beta_{eq}) + n_b P_3(s,\beta_{eq})}{P_4(s,\beta_{eq}) + n_b P_5(s,\beta_{eq})}, \quad (13)$$

where $s = \omega/q v_0$ is the phase velocity scaled by Fermi velocity, $\beta_{eq} = u_{eq}/v_0$ is the dimensionless velocity of electrons equilibrated with beam, $m_{hd} = \rho_{eq} v_0^2/n_{eq}$ and $m_b = 2n_{eq}/\partial n_{eq}/\partial\mu$ are the "proper" electron masses in hydrodynamic and ballistic regimes [27], and $P_i(s,\beta_{eq})$ are polynomial functions. To the leading order in beam density (and, hence,

drift velocity) they are given by

$$P_1 = 4s(1-2s^2)^2 - 4\beta_{\rm eq}(12s^4+8s^2-1), \quad (14)$$

$$P_2 = -4(4s^5-5s^3+s) + 6(6s^4-8s^2+1)\beta_{\rm eq}, \quad (15)$$

$$P_3 = -16s^5+20s^3+6s^2-4s-2, \quad (16)$$

$$P_4 = -32s^3+4\beta_{\rm eq}(26s^2-1), \quad (17)$$

$$P_5 = -8s^3-6s^2+1. \quad (18)$$

In the absence of electron beam, Eq. (13) readily reproduces the damping rate of equilibrium graphene plasmons [27]:

$$\gamma_0 = -\frac{qv_0{\rm Kn}}{8}\left[1+\left(\frac{m_{hd}}{m_b}-1\right)\left(\frac{1}{s}-2s\right)^2\right]. \quad (19)$$

The first term in square brackets is due to viscous damping. The second one can be traced down to the intrinsic conductivity of Dirac fluid [40–43] which, in turn, is a result of the nonconserved electric current upon collisions of Dirac electrons.

The beam effects on plasmon growth are proportional to the product of two small quantities, Knudsen number and relative density of beam electrons. It may be questioned whether beam can make a pronounced effect on damping compared to viscosity, the contribution of which is proportional to Kn solely. It appears that such a situation is possible in the limit of large wave phase velocity, $s \gg 1$. In this limit, the viscous damping disappears but the beam-induced growth persists, while the expression for the damping/growth rate acquires a simple form:

$$\gamma_{s\gg1} \approx -\frac{1}{2}qv_0s^2{\rm Kn}\left[\frac{m_{hd}}{m_b}-1-n_b\right]. \quad (20)$$

We observe therefore that beam-induced growth should compete only with damping due to intrinsic conductivity and not with the viscous damping. Further, in the limit of degenerate carriers, $\varepsilon_F/T \gg 1$, the last type of damping disappears, and the threshold density of beam electrons for onset of instability can be relatively small:

$$\frac{n_b}{n_0} \approx \frac{\pi^2}{3}\frac{T^2}{\varepsilon_F^2}. \quad (21)$$

The threshold beam density for the onset of plasma instability in the nearly hydrodynamic regime is a function of only two parameters: dimensionless phase velocity $s = \omega/qv_0$ and scaled Fermi energy. These universal dependences are shown in Fig. 3 with solid lines; dashed lines correspond to analytical low-temperature limits, Eq. (21). For small phase velocities $s \sim 1$, the threshold density becomes unachievably large as the beam-induced momentum transfer cannot compensate for viscous dissipation. At large velocities, the instability threshold abruptly goes to zero.

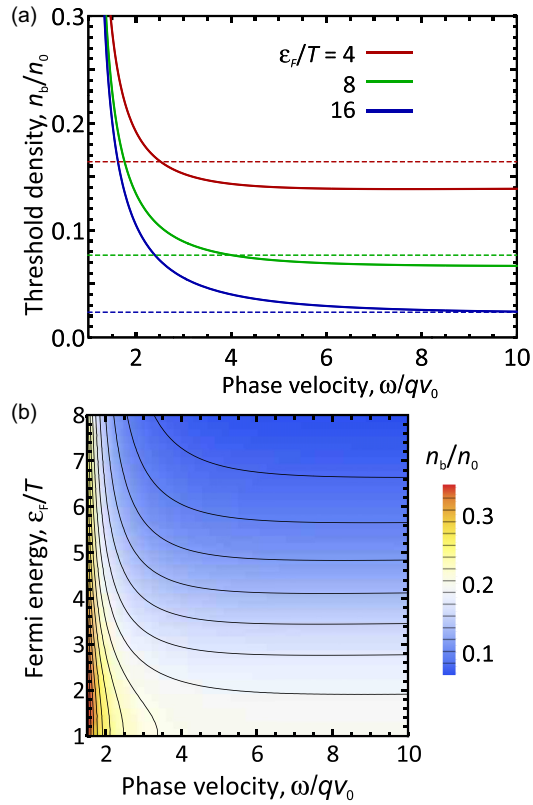

FIG. 3. Instability of normal graphene plasmons in the nearly hydrodynamic regime Kn $\ll 1$. Panel (a) shows the calculated threshold density of beam electrons for onset of instability vs wave velocity at various Fermi energy (solid lines). Dashed lines show an analytical approximation (21) to the threshold density. Panel (b) shows the color map of threshold density vs phase velocity s and Fermi energy ε_F/T.

IV. DISCUSSION AND CONCLUSIONS

We have revealed and theoretically studied two types of plasma instabilities in graphene induced by injection of collimated electron beam. The first one is associated with beam bunching, and appears for very weak electron-electron collisions. The second one is associated with viscous transfer of momentum from electron beam to collective plasmon modes, and appears at moderate strength of *e-e* collisions, $\omega\tau_{\rm ee} \sim 1$.

Emergence of both instabilities requires spatially dispersive (nonlocal) electromagnetic response. In the case of bunching instability, it is the nonlocal effect of Landau damping that gives rise to the growth of a lower beam-induced mode. We note that the bunching instability persists if polarizability is described within a simplified local model [25], but its characteristics are quite different from those obtained with the realistic model. Particularly, the local model predicts finite threshold density of beam electrons for instability onset, in contrast to thresholdless onset found with an account of Landau damping. The local model predicts the growth rate proportional to $n_b^{1/2}$, instead of linear growth rate $\propto n_b$ in the nonlocal model.

The above discussion was concentrated on stability of a spatially uniform distribution comprising steady electrons and collimated beam with energy slightly above the Fermi surface. This picture is simplified, as the beam electrons will undergo scattering and angular spreading upon propagation over the steady Fermi sea. Within the adopted model of

collision integral, the angular spreading would occur at length $l \sim v_0\tau_{ee}$. However, one can expect that the actual length of beam spreading would be longer.

First of all, the relaxation rates for even and odd harmonics of distribution function in two dimensions are different, $\tau_{\rm even} \approx \tau_{\rm ee} \approx (T/\varepsilon_F)^2\tau_{\rm odd}$ [44]. Due to this fact, the temporal evolution of beam features two characteristic steps [45]: (1) angular spreading of electrons across $\delta\theta \sim (T/\varepsilon_F)^{1/2}$ and formation of hole "tail" in the opposite direction during time $\tau_{\rm even}$; (2) complete angular equilibration during time $\tau_{\rm odd}$. We may suggest that spatial evolution of injected beam would also feature two characteristic lengths, $l_{\rm even} = v_0\tau_{\rm even}$ and $l_{\rm odd} = v_0\tau_{\rm odd}$. Stability study of "preequilibrium" beams with angular width $\delta\theta$ is a subject of foregoing research.

A second feature of slow angular spreading is peculiar for graphene and is associated with suppression of backscattering due to the chiral nature of carriers. As shown in recent pump-probe experiments [46], energy relaxation of hot carriers is almost unidirectional, with much slower angular diffusion. It is also possible to show that the presence of the beam itself weakly affects the electron relaxation time. This is primarily due to the small density of beam electrons $n_b/n_0 \ll 1$. Second, the collision of two electrons belonging to a well-collimated beam can lead only to a change in absolute values of carrier momenta, not their directions. Therefore, such interbeam collisions approximately preserve the angular collimation of the beam.

It is instructive to compare the criteria of stability for various distributions of drifting electrons. The above study conjectured that electron beam, a distribution of highest possible anisotropy, is unstable in the absence of collisions without any threshold in beam density. Another limiting case is locally equilibrium distribution of drifting electrons, which represents a Fermi distribution shifted by $\mathbf{k}\mathbf{u}_{\rm dr}$ in momentum space. Such patterns of drifting electrons can lead to instabilities in double-layer and grating-gated graphene, the velocity threshold being $u_{dr} \gtrsim v_0/\sqrt{2}$ [47]. High threshold velocity is paid off by insensitivity of hydrodynamic distributions to *e-e* collisions, while electron beams are strongly affected by the latter. The instability due to viscous momentum transfer from beam to normal plasmon modes is an appealing exception from this trade-off.

ACKNOWLEDGMENTS

This work was supported by Grants No. 18-37-20058 and No. 18-57-06001 of the Russian Foundation for Basic Research. The author thanks V. Ryzhii for helpful discussions and A. S. Petrov for proofreading of the manuscript.

APPENDIX A: EVALUATION OF POLARIZABILITY WITH QUANTUM KINETIC EQUATION

To derive the polarizability of background electrons Π_0 and beam Π_b, we start with a kinetic equation for electron density matrix $\rho = \rho_0 + \delta\rho$. Here $\delta\rho$ is the field-induced correction to the density matrix which varies in space and time as $e^{i\mathbf{q}\mathbf{r}-i\omega t}$; $\rho_0(\mathbf{k},\mathbf{k}') = \delta_{\mathbf{k},\mathbf{k}'}f_0(\mathbf{k}) \equiv \delta_{\mathbf{k},\mathbf{k}'}[f_F(k) + n_b\delta(\mathbf{k}-\mathbf{k}_b)]$ is the part of the density matrix unperturbed by field. It is represented by an equilibrium Fermi distribution part and collimated beam. The kinetic equation reads (we set $\hbar = 1$)

$$-i\omega\delta\rho = -i[\hat{H}_0, \delta\rho] - i[\hat{V}, \rho_0] - \gamma_{ee}(\delta\rho - \delta\rho_{eq}), \quad \text{(A1)}$$

where $\hat{H}_0$ is the Hamiltonian of free electrons, and the perturbation operator is represented by high-frequency field $V(\mathbf{k},\mathbf{k}') = -e\delta\varphi_{\mathbf{q}}\delta(\mathbf{k},\mathbf{k}+\mathbf{q})$. The relaxation term drives the perturbations of distribution function toward local equilibrium $\delta\rho_{eq}$ by conserving the number of particles, momentum, and energy (for an explicit form of the relaxation term in the quantum case, see [34]).

In the following, we shall ignore the two-band nature of electrons in graphene as we are ultimately interested in transition to the classical limit ($q \ll k_F$, $\omega \ll \varepsilon_F$). The only purpose of the quantum kinetic equation is to properly handle the highly singular distribution of beam electrons. The kinetic equation for density matrix (A1) is readily solved in a plane-wave basis; in momentum representation its only nonzero elements are those between $\mathbf{k}$ and $\mathbf{k}+\mathbf{q}$:

$$\delta\rho(\mathbf{k},\mathbf{k}+\mathbf{q}) = \frac{e\delta\varphi_{\mathbf{q}}[f_0(\mathbf{k}) - f_0(\mathbf{k}+\mathbf{q})] + i\gamma_{ee}\delta f_{eq}(\mathbf{k})}{\omega - \epsilon_{\mathbf{k}+\mathbf{q}} + \epsilon_{\mathbf{k}} + i\gamma_{ee}}. \quad \text{(A2)}$$

Above, $\delta f_{eq}(\mathbf{k})$ is the field-induced variation of the local-equilibrium distribution function:

$$\delta f_{eq}(\mathbf{k}) = \delta\mu_{eq}\partial_\mu f_{eq} + \delta\mathbf{u}_{eq}\partial_{\mathbf{u}} f_{eq} + \delta T_{eq}\partial_T f_{eq}. \quad \text{(A3)}$$

In the following, we will pass to the classical limit in all terms of (A2) not containing the singular beam distribution function, i.e., set

$$f_F(\mathbf{k}) - f_F(\mathbf{k}+\mathbf{q}) \approx -\mathbf{q}\frac{\partial f_F}{\partial \mathbf{k}}, \quad \epsilon_{\mathbf{k}} - \epsilon_{\mathbf{k}+\mathbf{q}} \approx -\mathbf{q}\mathbf{v}_{\mathbf{k}}. \quad \text{(A4)}$$

The density matrix (and distribution functions) of noninteracting particles ($\gamma_{ee} \to 0$) are additive. In other words, they can be represented as sums of those due to background electrons and the beam, namely

$$\delta\rho(\mathbf{k},\mathbf{k}+\mathbf{q}) = e\delta\varphi_{\mathbf{q}}\frac{-\mathbf{q}\partial f_F/\partial\mathbf{k}}{\omega - \mathbf{q}\mathbf{v}_{\mathbf{k}} + i0} + e\delta\varphi_{\mathbf{q}}n_b\frac{\delta(\mathbf{k}-\mathbf{k}_b) - \delta(\mathbf{k}+\mathbf{q}-\mathbf{k}_b)}{\omega - \epsilon_{\mathbf{k}+\mathbf{q}} + \epsilon_{\mathbf{k}} + i0}. \quad \text{(A5)}$$

Knowing the density matrix, one finds the field-induced electron density $\delta n_q = \sum_{\mathbf{k}}\delta\rho(\mathbf{k},\mathbf{k}+\mathbf{q})$ and the polarizability $\delta n_q = \Pi(\mathbf{q},\omega)e\delta\varphi_{\mathbf{q}}$. In accordance with decomposition (A5), the polarizability is presented as

$$\Pi(\mathbf{q},\omega) = \Pi_0(\mathbf{q},\omega) + \Pi_b(\mathbf{q},\omega), \quad \text{(A6)}$$

$$\Pi_0(\mathbf{q},\omega) = -\sum_{\mathbf{k}}\frac{\mathbf{q}\partial f_F/\partial\mathbf{k}}{\omega - \mathbf{q}\mathbf{v}_{\mathbf{k}} + i0} = \frac{2}{\pi}\frac{k_F}{v_0}\left[1 - \frac{\omega}{\sqrt{(\omega+i0)^2 - q^2v_0^2}}\right], \quad \text{(A7)}$$

$$\Pi_b(\mathbf{q},\omega) = n_b\sum_{\mathbf{k}}\frac{\delta(\mathbf{k}-\mathbf{k}_b) - \delta(\mathbf{k}+\mathbf{q}-\mathbf{k}_b)}{\omega - \epsilon_{\mathbf{k}+\mathbf{q}} + \epsilon_{\mathbf{k}} + i0} = n_b\left[\frac{1}{\omega - \epsilon_{\mathbf{k}_b+\mathbf{q}} + \epsilon_{\mathbf{k}_b}} - \frac{1}{\omega - \epsilon_{\mathbf{k}_b} + \epsilon_{\mathbf{k}_b-\mathbf{q}}}\right]. \quad \text{(A8)}$$

Going beyond the classical limit is important in the energy denominators of the beam polarizability. One can approximate

$$\epsilon_{\mathbf{k_b}+\mathbf{q}} - \epsilon_{\mathbf{k_b}} \approx \mathbf{q}\mathbf{v_b} - qv_0 \sin^2\theta \frac{q}{2k_b}, \tag{A9}$$

$$\epsilon_{\mathbf{k_b}} - \epsilon_{\mathbf{k_b}-\mathbf{q}} \approx \mathbf{q}\mathbf{v_b} + qv_0 \sin^2\theta \frac{q}{2k_b}, \tag{A10}$$

where $\mathbf{v_b} = v_0\mathbf{k}_0/k_0$ is the velocity of beam electrons and θ is the angle between beam and plasmon propagation direction. Expressions (A8) for beam polarizability and expansions (A9) and (A10) justify the form of polarizability (10) used in the main text:

$$\Pi_b = n_b\left[\omega - \mathbf{q}\mathbf{v_b} + qv_0 \sin^2\theta \frac{q}{2k_b}\right]^{-1} - n_b\left[\omega - \mathbf{q}\mathbf{v_b} - qv_0 \sin^2\theta \frac{q}{2k_b}\right]^{-1}. \tag{A11}$$

We can perform an explicit subtraction in (A11) and neglect a small difference in denominators. We shall arrive therefore at the polarizability $\tilde{\Pi}_b$ used in Ref. [25]:

$$\tilde{\Pi}_b = -n_b \frac{qv_0 \sin^2\theta q/k_b}{(\omega - \mathbf{q}\mathbf{v_b})^2}. \tag{A12}$$

The latter equation does not capture the splitting of beam-induced modes clearly seen in calculated dispersions [Figs. 1(a) and 1(b)]. It can be applicable only at large densities of beam electrons $n_b/n_0 \gg q/k_b$.

APPENDIX B: GENERALIZED HYDRODYNAMIC EQUATIONS

We repeat the derivation steps of generalized hydrodynamic equations that enable one to find the parameters of local equilibrium distribution function $\delta\mu$, $\delta\mathbf{u}$, δT at given external potential $\delta\varphi$. The details can be found in [47]. The derivation is based on conservation of particle number, momentum, and energy upon *e-e* collisions. These conservation laws can be symbolically presented as

$$\sum_{\mathbf{k}} \mathbf{g_k} \mathcal{C}_{ee}\{\delta f(\mathbf{k})\} = 0, \tag{B1}$$

where $\mathbf{g_k} = \{1, \mathbf{k}, \varepsilon_{\mathbf{k}}\}$ is the vector of conserved quantities. With model integral of *e-e* collisions (3), the above requirement simplifies to

$$\sum_{\mathbf{k}} \mathbf{g_k}[\delta f(\mathbf{k}) - \delta f_{eq}(\mathbf{k})] = 0, \tag{B2}$$

where $\delta f(\mathbf{k})$ is given by (5) and $\delta f_{eq}(\mathbf{k})$ by Eq. (7). Upon performing integration over momentum space, we are led to a system of generalized hydrodynamic equations.

Formulation of this system in terms of $\delta\mu$, $\delta\mathbf{u}$, and δT is inconvenient. Instead, we pass to the variations of particle density δn, relativistic velocity $\delta\beta = \delta u/v_0$, and mass density $\delta\rho$. These variations are bound by equations of state:

$$\delta n = \frac{\partial n}{\partial \mu}\delta\mu + \frac{3\beta n}{1-\beta^2}\delta\beta + \frac{2n - \mu\partial n/\partial\mu}{T}\delta T, \tag{B3}$$

$$\delta\rho = (\rho - \mu n/v_0^2)\frac{3\delta T}{T} + \frac{5\beta\rho}{1-\beta^2}\delta\beta. \tag{B4}$$

Introducing the vector of unknown quantities $\mathbf{x} = \{\delta n/n, \delta\beta, \delta\rho/\rho\}$, we can formulate the generalized hydrodynamic equations in a symbolic matrix form

$$\hat{M}\mathbf{x} = \mathbf{f}_{pl} + \mathbf{f}_b, \tag{B5}$$

where $\mathbf{f}_{pl}$ and $\mathbf{f}_b$ can be considered as generalized forces acting on background electron plasma and electron beam. The hydrodynamic matrix has the form

$$\hat{M} = \begin{pmatrix} 1 - i\tilde{\gamma}_{ee}J_{02} & -i\tilde{\gamma}_{ee}\partial_\beta J_{02} & 0 \\ 0 & 1 - \frac{2i}{3}\tilde{\gamma}_{ee}\partial_\beta J_{13} & \beta_{eq} - \frac{2i}{3}\tilde{\gamma}_{ee}J_{13} \\ 0 & \beta_{eq} - i\tilde{\gamma}_{ee}\partial_\beta J_{03} & 1 - i\tilde{\gamma}_{ee}J_{03} \end{pmatrix}, \tag{B6}$$

where we have introduced the dimensionless strength of *e-e* collisions $\tilde{\gamma}_{ee} = (qv_0\tau)^{-1} = \mathrm{Kn}^{-1}$. The dimensionless quantities J_{nm} depend only on equilibrium velocity β_{eq} and ratio $a = (\omega + i\gamma_{ee})/qv_0$:

$$J_{nm}(a,\beta) = \frac{(1-\beta^2)^{m-\frac{1}{2}}}{2\pi}\int_0^{2\pi} \frac{\cos^n\theta\, d\theta}{(1-\beta\,\cos\theta)^m(a - \cos\theta)}. \tag{B7}$$

The force vectors have the form

$$\mathbf{f}_{pl} = -2\begin{pmatrix} \frac{J_{10}}{m_k v_0^2} \\ \frac{J_{20}}{m_{hd} v_0^2} \\ \frac{3J_{10}/2}{m_{hd} v_0^2} \end{pmatrix}, \tag{B8}$$

$$\mathbf{f}_b = \frac{n_b}{n}\begin{pmatrix} \frac{1}{\omega+i\gamma_{ee}-\omega_b^-} - \frac{1}{\omega+i\gamma_{ee}-\omega_b^+} \\ \frac{1}{m_{hd}v_0^2}\left(\frac{k_b v_0\cos\theta}{\omega+i\gamma_{ee}-\omega_b^-} - \frac{k_b v_0\cos\theta + qv_0}{\omega+i\gamma_{ee}-\omega_b^+}\right) \\ \frac{1}{2m_{hd}v_0^2/3}\left(\frac{\varepsilon_{k_b}}{\omega+i\gamma_{ee}-\omega_b^-} - \frac{\varepsilon_{k_b+q}}{\omega+i\gamma_{ee}-\omega_b^+}\right) \end{pmatrix}, \tag{B9}$$

where we have introduced 'kinetic' and 'hydrodynamic' masses of carriers in graphene, $m_k = 2n/(v_0^2\partial n/\partial\mu)$ and $m_{hd} = \rho/n$. Though quite tedious, the system enables a full analytical treatment at arbitrary *e-e* collision frequency.

APPENDIX C: MAXIMUM ACHIEVABLE GROWTH RATE OF BEAM INSTABILITY

In this section, we maximize the growth rate of beam instability with respect to wave vector q, propagation angle θ, and Coulomb coupling strength α_c. We shall assume $k_b \approx k_F$ as the energy of a beam is quickly relaxed, while angular spreading can be relatively slow. To perform maximization, we introduce the dimensionless wave vector $\tilde{q} = q/k_b$, and rewrite Eq. (12) for the lowest mode as

$$\frac{\omega_b^-}{\varepsilon_F} = \tilde{q}\,\cos\theta - \tilde{q}|\sin\theta|\left[\left(\frac{\tilde{q}\,\sin\theta}{2}\right)^2 + \frac{p_b\alpha_c}{\tilde{q} + 4\alpha_c F(s)}\right]^{1/2}, \tag{C1}$$

$$F(s) = 1 + \frac{is}{\sqrt{1-s^2}}. \tag{C2}$$

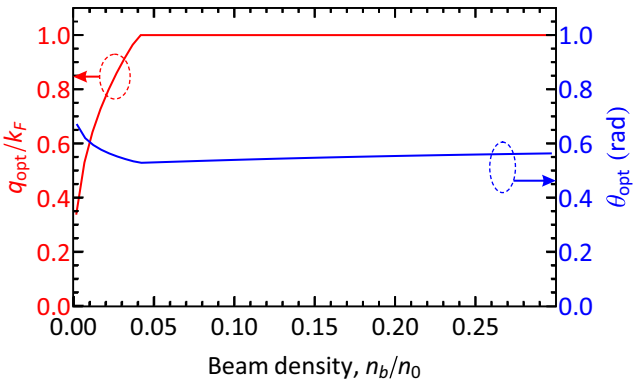

FIG. 4. Values of wave propagation angle with respect to the beam θ and wave vector q/k_F delivering the maximum for the instability growth rate. The wave vector is constrained below k_F to guarantee the validity of quasiclassical approximation.

The function $F(s)$ depends only on mode phase velocity $s = \omega/qv_0$. For the lowest beam mode, we can approximate $s \approx \cos\theta - (\tilde{q}/2)\sin^2\theta$.

Imaginary part (growth rate) of beam mode frequency (C1) is a continuously growing function of α_c; therefore, we constrain α_c to its maximum possible value for suspended graphene $\alpha_c \approx 2.2$. With variation of $\tilde{q}$, the growth rate has a maximum which can be achieved both below and above k_F. To stay within the applicability of quasiclassical approximation, we restrict $q < k_F$ ($\tilde{q} < 1$). Finally, with variation of angle, the growth rate achieves a maximum in the vicinity of $\theta \sim \pi/5$.

The result of constrained optimization of Eq. (C1) with respect to the remaining two variables is shown in Fig. 1(c). The values of angle and wave vector delivering the optimum for growth rate, θ_{opt} and q_{opt}, are shown in Fig. 4.

[1] A. A. Abrikosov and I. M. Khalatnikov, Rep. Prog. Phys. **22**, 329 (1959).
[2] J. Voit, Rep. Prog. Phys. **58**, 977 (1995).
[3] A. Chaplik, Sov. Phys. JETP **33**, 997 (1971).
[4] A. Shytov, J. F. Kong, G. Falkovich, and L. Levitov, Phys. Rev. Lett. **121**, 176805 (2018).
[5] A. D. Levin, G. M. Gusev, E. V. Levinson, Z. D. Kvon, and A. K. Bakarov, Phys. Rev. B **97**, 245308 (2018).
[6] R. K. Kumar, D. Bandurin, F. Pellegrino, Y. Cao, A. Principi, H. Guo, G. Auton, M. B. Shalom, L. A. Ponomarenko, G. Falkovich *et al.*, Nat. Phys. **13**, 1182 (2017).
[7] D. A. Bandurin, I. Torre, R. K. Kumar, M. Ben Shalom, A. Tomadin, A. Principi, G. H. Auton, E. Khestanova, K. S. Novoselov, I. V. Grigorieva, L. A. Ponomarenko, A. K. Geim, and M. Polini, Science **351**, 1055 (2016).
[8] J. Gooth, F. Menges, N. Kumar, V. Süß, C. Shekhar, Y. Sun, U. Drechsler, R. Zierold, C. Felser, and B. Gotsmann, Nat. Commun. **9**, 4093 (2018).
[9] A. I. Akhiezer and Y. B. Fainberg, Dokl. Akad. Nauk SSSR **69**, 555 (1949) [Ukrainean Journal of Physics **53**, 87 (2008)].
[10] E. Lifshits and L. Pitaevskii, *Physical Kinetics*, Course of Theoretical Physics (North-Holland, Amsterdam, 1981).
[11] J. Neufeld and P. H. Doyle, Phys. Rev. **121**, 654 (1961).
[12] V. Parail and O. Pogutse, Nucl. Fusion **18**, 303 (1978).
[13] V. Ginzburg and V. Zhelezniakov, Sov. Astron. **2**, 653 (1958).
[14] H. Predel, H. Buhmann, L. W. Molenkamp, R. N. Gurzhi, A. N. Kalinenko, A. I. Kopeliovich, and A. V. Yanovsky, Phys. Rev. B **62**, 2057 (2000).
[15] A. Yanovsky, H. Predel, H. Buhmann, R. Gurzhi, A. Kalinenko, A. Kopeliovich, and L. Molenkamp, Europhys. Lett. **56**, 709 (2001).
[16] M. P. Jura, M. Grobis, M. A. Topinka, L. N. Pfeiffer, K. W. West, and D. Goldhaber-Gordon, Phys. Rev. B **82**, 155328 (2010).
[17] M. A. Topinka, B. J. LeRoy, S. E. J. Shaw, E. J. Heller, R. M. Westervelt, K. D. Maranowski, and A. C. Gossard, Science **289**, 2323 (2000).
[18] M. Heiblum, M. I. Nathan, D. C. Thomas, and C. M. Knoedler, Phys. Rev. Lett. **55**, 2200 (1985).
[19] K. Kempa, P. Bakshi, J. Cen, and H. Xie, Phys. Rev. B **43**, 9273 (1991).
[20] E. Starikov, V. Gružinskis, and P. Shiktorov, Phys. Status Solidi A **190**, 287 (2002).
[21] B. Y.-K. Hu and J. W. Wilkins, Phys. Rev. B **43**, 14009 (1991).
[22] A. N. Korshak, Z. S. Gribnikov, N. Z. Vagidov, and V. V. Mitin, Appl. Phys. Lett. **75**, 2292 (1999).
[23] V. Gruzinskis, R. Mickevičius, J. Pozela, and A. Reklaitis, Europhys. Lett. **5**, 339 (1988).
[24] The Dyakonov-Shur instability is an example of instabilities favored by highly collisional hydrodynamic transport. Reduction of *e-e* collision frequency increases viscosity and suppresses such instability.
[25] C. M. Aryal, B. Y.-K. Hu, and A.-P. Jauho, Phys. Rev. B **94**, 115401 (2016).
[26] P. L. Bhatnagar, E. P. Gross, and M. Krook, Phys. Rev. **94**, 511 (1954).
[27] D. Svintsov, Phys. Rev. B **97**, 121405(R) (2018).
[28] A. A. Rukhadze and V. P. Silin, Sov. Phys. Usp. **11**, 659 (1969).
[29] D. Y. H. Ho, I. Yudhistira, N. Chakraborty, and S. Adam, Phys. Rev. B **97**, 121404(R) (2018).
[30] V. V. Cheianov and V. I. Fal'ko, Phys. Rev. B **74**, 041403(R) (2006).
[31] S. Chen, Z. Han, M. M. Elahi, K. M. M. Habib, L. Wang, B. Wen, Y. Gao, T. Taniguchi, K. Watanabe, J. Hone, A. W. Ghosh, and C. R. Dean, Science **353**, 1522 (2016).
[32] S. Bhandari, G. H. Lee, K. Watanabe, T. Taniguchi, P. Kim, and R. M. Westervelt, 2D Mater. **5**, 021003 (2018).
[33] A. W. Barnard, A. Hughes, A. L. Sharpe, K. Watanabe, T. Taniguchi, and D. Goldhaber-Gordon, Nat. Commun. **8**, 1 (2017).
[34] G. S. Atwal and N. W. Ashcroft, Phys. Rev. B **65**, 115109 (2002).
[35] V. Ryzhii, Jpn. J. Appl. Phys. **45**, L923 (2006).
[36] M. B. Lundeberg, Y. Gao, R. Asgari, C. Tan, B. Van Duppen, M. Autore, P. Alonso-González, A. Woessner, K. Watanabe,

T. Taniguchi, R. Hillenbrand, J. Hone, M. Polini, and F. H. L. Koppens, Science **357**, 187 (2017).
[37] D. Svintsov and V. Ryzhii, Phys. Rev. Lett. **123**, 219401 (2019).
[38] A. B. Mikhailovskii, *Theory of Plasma Instabilities. Volume 1: Instabilities of a Homogeneous Plasma* (Springer Science+Business Media, New York, 1974).
[39] D. Svintsov, V. Vyurkov, S. Yurchenko, T. Otsuji, and V. Ryzhii, J. Appl. Phys. **111**, 083715 (2012).
[40] P. Gallagher, C.-S. Yang, T. Lyu, F. Tian, R. Kou, H. Zhang, K. Watanabe, T. Taniguchi, and F. Wang, Science **364**, 158 (2019).
[41] L. Fritz, J. Schmalian, M. Müller, and S. Sachdev, Phys. Rev. B **78**, 085416 (2008).
[42] A. Lucas, Phys. Rev. B **93**, 245153 (2016).
[43] A. Principi, G. Vignale, M. Carrega, and M. Polini, Phys. Rev. B **88**, 195405 (2013).
[44] R. N. Gurzhi, A. N. Kalinenko, and A. I. Kopeliovich, Phys. Rev. Lett. **74**, 3872 (1995).
[45] R. N. Gurzhi, A. N. Kalinenko, and A. I. Kopeliovich, Phys. Rev. B **52**, 4744 (1995).
[46] J. C. König-Otto, M. Mittendorff, T. Winzer, F. Kadi, E. Malic, A. Knorr, C. Berger, W. A. de Heer, A. Pashkin, H. Schneider, M. Helm, and S. Winnerl, Phys. Rev. Lett. **117**, 087401 (2016).
[47] D. Svintsov, Phys. Rev. B **100**, 195428 (2019).